Mineralogical Magazine, October 2016, Vol. 80(6), pp. 959–975

Water incorporation in garnets from ultrahigh pressure eclogites at Shuanghe, Dabieshan

Xiang-Wen Liu[1,2,*], Zhan-Jun Xie[3,4], Lu Wang[2], Wei Xu[4] and Zhen-Min Jin[3]

[1] Engineering Research Center of Nano-Geo Materials of Ministry of Education, China University of Geosciences, Wuhan, 430074, P.R. China
[2] State Key Laboratory of Geological Processes and Mineral Resources, China University of Geosciences, Wuhan, 430074, P.R. China
[3] Faculty of Earth Sciences, China University of Geosciences, Wuhan, 430074, P.R. China;
[4] East China Mineral Exploration and Development Bureau for Non-Ferrous, Nanjing, 210007, P.R. China

[*Received 12 January 2015; Accepted 16 September 2015; Associate Editor: Ed Grew*]

ABSTRACT

The hydrogen concentration and composition of garnets in the ultrahigh pressure eclogites at Shuanghe, eastern Dabieshan, were investigated using Fourier transform infrared spectroscopy and electron microprobe analysis. The OH absorption bands can be divided into four groups: (1) 3635–3655 cm^{-1}; (2) 3600–3630 cm^{-1}; (3) 3540–3580 cm^{-1}; and (4) 3400–3450 cm^{-1} and the water content ranges from 45 to 2529 ppm. Based on the behaviour of the OH absorption band and the relationship between water content and the composition of garnets, the samples can be divided into two classes: samples with >400 ppm H_2O and samples with ≤400 ppm H_2O. The water content of the former shows an obvious positive correlation with Ca atoms and a negative correlation with the Si, Mg and Fe^{2+} atoms per 12 anions, whereas the water content of the latter shows no obvious linear correlation with cations. It is concluded that the major mechanism of hydroxyl incorporation in garnets with >400 ppm H_2O is by the coupled substitution $4H + {}^{Z}\square \rightarrow \square + {}^{Z}Si$ in the tetrahedral site, and that several mechanisms are responsible for OH incorporation in garnets with ≤400 ppm H_2O.

Keywords: Dabieshan, Shuanghe, ultrahigh pressure eclogite, garnet, water incorporation.

Introduction

Since the 1960–70s, it has been shown that almost all nominally anhydrous minerals (NAMs) such as quartz, garnet, pyroxene, olivine, and their high-pressure phases contain small amounts of hydrogen in the crystal defects, present as OH^- groups or H_2O molecules, and water content ranges from <1 ppm to several thousand ppm (Martin and Donnay, 1972; Wilkins and Sabine, 1973; Rossman, 1996; Keppler and Smyth, 2006; Steven and Suzan, 2006; Geiger, 2013). As the major mineral in eclogite and other metamorphic rocks, garnet is an important subject in studying the water of NAMs; it has been found that hydrogen is an element in some approved species of garnet (such as katoite, holtstamite and henritermierite) (Armbruster *et al.*, 2001; Ferro *et al.*, 2003; Hålenius *et al.*, 2005). Due to the complexity of its composition and its stability over a wide range of pressures and temperatures, the mechanisms of OH incorporation in garnet are not yet well understood (Ingrin and Skogby, 2000; Beran and Libowitzky, 2003, 2006; Johnson, 2006; Libowitzky and Beran, 2006). The composition and crystal structure of garnet can significantly influence the OH incorporation mechanism and its content. In hydrous garnets, the major mechanism of hydroxyl incorporation is by the coupled substitution $4H + {}^{Z}\square \rightarrow \square + {}^{Z}Si$, i.e. the hydrogen ions occupy a separate site of general symmetry (Wyckoff position 96*h*) coordinated to the 4 O coordinated originally to Si, which is

*E-mail: xwliu@cug.edu.cn
DOI: 10.1180/minmag.2016.080.034

absent. The hydrogen ion has been investigated by Fourier transform infrared (FTIR) spectroscopy, nuclear reaction analysis (NRA), neutron magnetic resonance (NMR), as well as by neutron and X-ray diffraction and by computer simulation (Foreman, 1968; Aines and Rossman, 1984*a*; Lager *et al.*, 1987, 1989; Beran *et al.*, 1993; Cho and Rossman, 1993; Wright *et al.*, 1994; Milman *et al.*, 2000; Maldener *et al.*, 2003; Beran and Libowitzky, 2006; Wright, 2006; Grew *et al.*, 2013). However, most natural garnet contains much less H_2O, and their IR spectra are more complex, which suggests that OH groups have been incorporated by mechanisms other than $4H + {}^{Z}\square \rightarrow \square + {}^{Z}Si$ (Birkett and Trzcienski, 1984; Kalinichenko *et al.*, 1987; Geiger *et al.*, 1991; Khomenko *et al.*, 1994; Lu and Keppler, 1997; Armbruster *et al.*, 1998; Ingrin and Skogby, 2000; Andrut and Wildner, 2001; Andrut *et al.*, 2002; Johnson, 2003; Beran and Libowitzky, 2003; Blanchard and Ingrin, 2004; Kurka *et al.*, 2005).

As in the previous studies, the water content of garnet from the ultrahigh-pressure (UHP) eclogites in eastern Dabieshan showed a large variation, ranging from <100 ppm to >1800 ppm, and the OH incorporation mechanism is not yet well understood (Zhang *et al.*, 2001; Sheng *et al.*, 2005; Xia *et al.*, 2005). In this paper, we report our investigations by FTIR and electron microprobe analysis (EMPA) of the relationship between hydrogen concentration and composition of garnet from the UHP eclogites in Shuanghe, eastern Dabieshan.

Geological background and sample description

The Dabie-Sulu orogenic belt in China is the largest (>30,000 km^2) and one of the best-exposed UHP metamorphic terranes known. Numerous studies have shown that this belt resulted from the subduction of the South China Block beneath the North China Block followed by rapid exhumation (Zheng, 2008; Zhang *et al.*, 2009) during the Mesozoic. The Dabie orogen is located in central-eastern China, and it is bounded by the strike-slip Tan-Lu (Tancheng-Lujiang) fault with the Sulu belt to the east, and it connects with the Qinling orogen in the west (Fig. 1*a*). From north to south, the Dabie Block is divided into: (I) a low-grade metamorphic belt; (II) the north Dabie high-T/P amphibolite/granulite belt; and (III) the central Dabie UHP belt. The UHP belt grades southwards to a narrow coesite-free eclogite belt (IV); and there is an epidote amphibolites + narrow blueschist belt (V) along the southern margin of the Dabie Block (Zhang *et al.*, 2009).

In this study, ten eclogite samples were collected from Shuanghe UHP metamorphic rocks of the central Dabie UHP belt (Fig. 1*b*). Eclogites crop out either within orthogneisses (Shw2, Shx1 and Shx4) and marbles (Shx7, Shx8, Shx9 and Shx13) or together with UHP jadeite quartzite (Shx15, Shx17 and Shx18). They are preserved as folded layers and lenses in the epidote two-mica schist and also as folded lenses and smaller nodules in the marble. The age of peak metamorphism is ~220–230 Ma, when $P > \sim$27–28 kbar and $T = 700 \pm 50$°C (Cong *et al.*, 1995; Liou *et al.*, 1997; Li *et al.*, 2000; Liu *et al.*, 2006; Wang *et al.*, 2010). Most of the Shuanghe eclogites are foliated, and the UHP minerals such as garnet, omphacite and rutile are stretched substantialy. The critical temperature (lower limit for ductile deformation) under which plastic deformation of garnets took place is estimated to correspond to the coesite eclogite phase condition (Xu *et al.*, 1999, 2008; Liu *et al.*, 2005, 2006).

In this study, the samples of Shx1, Shx7, Shx8, Shx9 and Shx13 are strongly retrograded (Fig. 2*a*), consisting of large garnet porphyroblasts set in a matrix of finer-grained amphibole, quartz and plagioclase. Nearly all of the omphacites have been replaced by symplectites of Ca-pyroxene and/or Ca-amphibole with sodic plagioclase. In contrast, the sample of Shw2, Shx4, Shx15, Shx17 and Shx18 are fresh or slightly retrograded (Fig. 2*b*), and the garnet and omphacite are coarse-grained and equigranular in texture. The garnets investigated are large crystals that are free of visible cracks and inclusions under the microscope.

Analytical methods

Double-sided polished chips ~2 cm × 1 cm in area and ~0.2–0.4 mm thick were prepared. Because the precision of measuring thickness by micrometer of the chips is <10% at any one point, the average of more than 35 points obtained from measurements over the entire chip was applied to individual grains in the chip (Table 1, and Supplementary file 1. Supplementary files have been deposited with the Principal Editor of *Mineralogical Magazine* and are available from www.minersoc.org/pages/e-journals/dep_mat_mm.html). The cleaning procedure included >8 h of dissolution of the chips in ethanol or acetone, followed by repeated cleaning with ethanol and distilled water. To remove the surface-

https://doi.org/10.1180/minmag.2016.080.034 Published online by Cambridge University Press

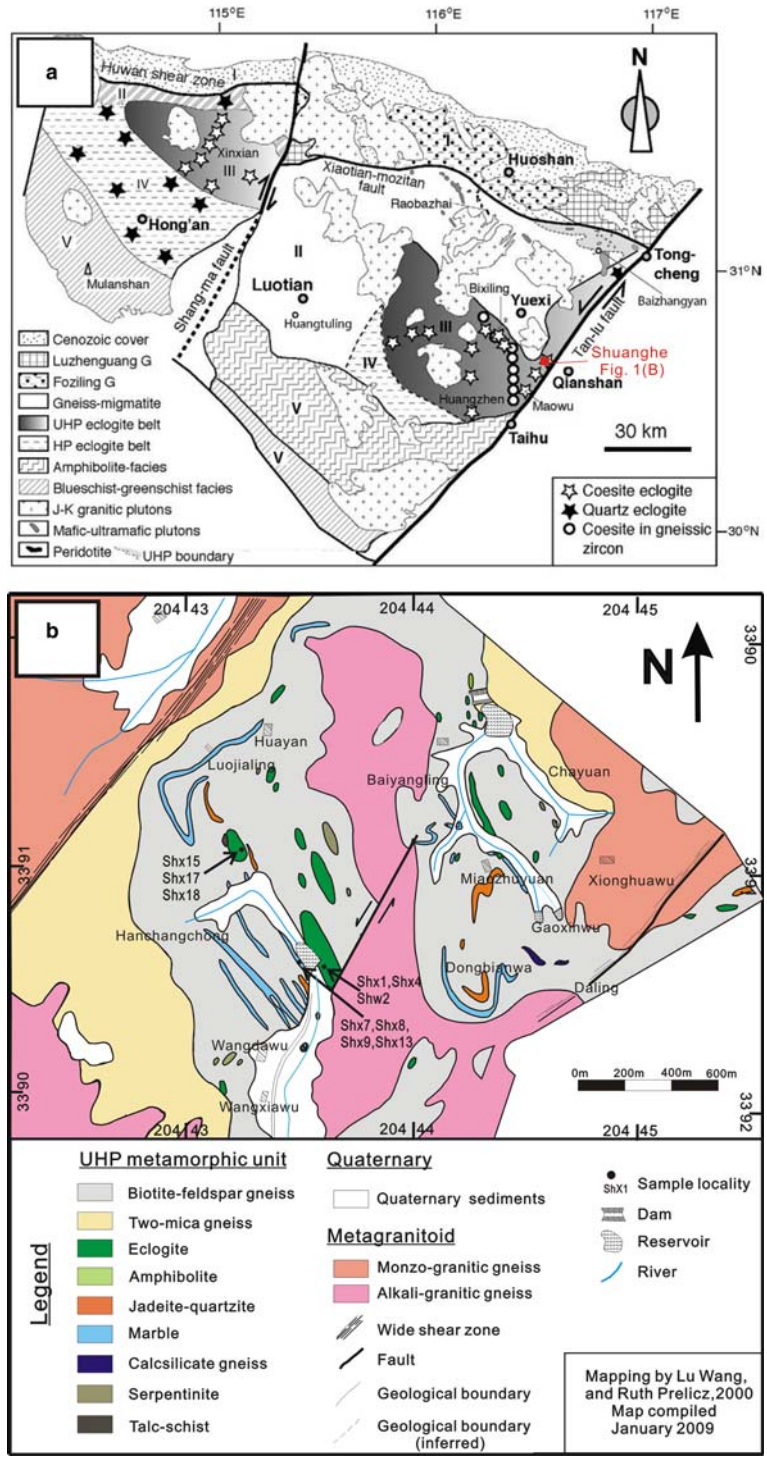

FIG. 1. (*a*) General geological and tectonic map of the Dabie Mountains (modified after Zhang, *et al.* 2009); (*b*) Geological map of Shuanghang area, Pailou, Anhui Province (modified after Wang *et al.* 2010).

https://doi.org/10.1180/minmag.2016.080.034 Published online by Cambridge University Press

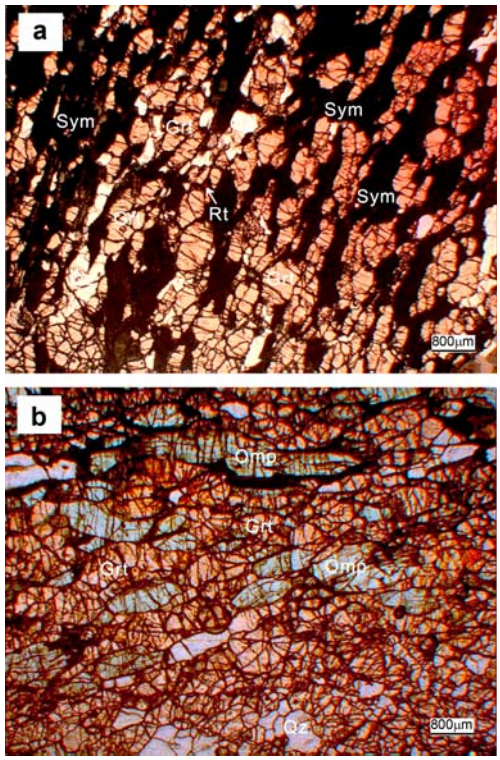

FIG. 2. Photomicrographs of the eclogites. (*a*) Retrograded eclogite of sample Shx1; (*b*) fresh eclogite of sample Shx17. (Grt, garnet; Omp, omphacite; Qz, quartz; Rt, rutile; Sym, symplectite. All the photographs were taken under plane polarized light).

absorbed water, the thin chips were heated for >6 h in an oven at ~110°C. Infrared spectra were obtained at room temperature in the range 650–4000 cm^{-1} on a Nicolet 6700 FTIR spectrometer at the State Key Laboratory of Geological Process and Mineral Resources, China University of Geosciences, Wuhan, China. Measurements were carried out with unpolarized radiation with an IR light source, a KBr beam-splitter, and an MCT-A liquid N_2-cooled detector. For each analysis, 128 scans at a resolution of 4 cm^{-1} were recorded.

The compositions of all samples were determined using EMPA on the JEOL JXA-733 electron probe at the State Key Laboratory of Geological Process and Mineral Resources, China University of Geosciences, Wuhan, China. Measurements were carried out at 15 kV accelerating voltage, 20 nA beam current, 10 μm electron beam diameter and 20 s count times on the peaks. The EMPA standards include the following minerals: jadeite for Na, ilmenite for Ti and Fe, K-feldspar for K, wollastonite for Si and Ca, MgO for Mg, Al_2O_3 for Al, $MnSiO_3$ for Mn and Cr_2O_3 for Cr. In order to check the accuracy of our EMPA data, duplicate analyses were performed on five samples (Shw2, Shx1, Shx4, Shx7, Shx13) with another electron probe, a JEOL JXA-8230 at the Center of Testing and Analysis, Wuhan University of Technology, Wuhan, China, using 15 kV accelerating voltage, 20 nA beam current and 5 μm electron beam diameter. The following standards were used: $NaAlSi_2O_6$ for Na, $(Mg, Fe)_2SiO_4$ for Mg, $KAlSi_3O_8$ for K, $MgCaSi_2O_6$ for Ca, TiO_2 for Ti, $Fe_3Al_2Si_3O_{12}$ for Al, $MgCaSi_2O_6$ for Si, Cr_2O_3 for Cr, $(Mn, Ca)SiO_3$ for Mn, $Fe_3Al_2Si_3O_{12}$ for Fe. The results (Supplementary file 2) are consistent with our analysis using the JEOL JXA-733 (Table 2, Supplementary file 3) and previous research (Cong *et al.*, 1995; Wang *et al.*, 2010). Formulae were calculated by the Excel spreadsheet that Grew *et al.* (2013) recommended, and most Si contents are still >3 atoms per formula unit (apfu).

FTIR analysis results

The FTIR spectrum of the 22 garnet grains investigated (91 spots) show at least two absorption bands in the typical OH-stretching vibration region of ~3000–3800 cm^{-1} (Fig. 3*a*,*b*; Table 1). The broad absorption rising towards higher wavenumbers is due to an electronic transition in Fe^{2+} (Aines and Rossman, 1984*b*; Bell and Rossman, 1992), and the weak band at ~3710 cm^{-1} in some spectra is probably due to contamination from water vapour in air. After background correction, the spectra were resolved into Gaussian- and Lorentzian-shaped absorption bands, and their band centre, their full width at half-height (FWHH), and their integral intensity were determined with the software of *PeakFit V4.12* by Jandel Scientific (Andrut *et al.*, 2002). The OH-absorption bands can be divided into four groups: (I) 3635–3655 cm^{-1}; (II) 3600–3630 cm^{-1}; (III) 3540–3580 cm^{-1}; and (IV)) 3400–3450 cm^{-1} (Table 1, Supplementary file 4; Fig. 3*c*,*d*). The position of the first three groups of bands are in the energy range (generally 3500–3700 cm^{-1}) of structural OH^-, and are composed of relatively sharp bands with FWHH<160 cm^{-1}. They are considered to be the result of OH-vibrations of the tetrahedral site in garnet similiar to those observed in hydrogrossular (Aines and Rossman, 1984*a*; Birkett and Trzcienski, 1984; Rossman and Aines, 1991; Cho

https://doi.org/10.1180/minmag.2016.080.034 Published online by Cambridge University Press

TABLE 1. FTIR analysis of garnets from UHP eclogites at Shuanghe, Dabieshan.

			Group I		Group II		Group III		Group IV		
			3635–3655 cm^{-1}		3600–3630 cm^{-1}		3540–3580 cm^{-1}		3400–3450 cm^{-1}		
Sample	Thickness (mm)	Spot	FWHH	Area	FWHH	Area	FWHH	Area	FWHH	Area	Water Content (ppm)
Shw2	0.334	g1–1	34	1.18	71	3.01					90
		g1-2	37	1.68	54	2.05	31	0.11			83
		g1-3	38	2.07	48	1.57	40	0.09			80
		g1-4	38	2.09	46	1.49	104	0.70			92
Shx1	0.284	g1-1	34	0.75	50	0.91	28	0.12			45
		g1-2	35	0.69	52	0.85	39	0.25			45
		g2-1 (C)	39	1.15	36	0.76	80	2.47	126	1.29	111
		g2-2 (M)	38	0.93	32	0.47	103	3.26	133	1.11	118
		g2-3 (M)	38	0.76	37	0.40	102	2.67	130	1.37	97
		g2-4 (R)			97	8.00	79	7.70	221	26.55	398
		g2-5 (R)	50	2.41			88	9.74	203	17.74	308
		g2-6 (R)	34	0.97	35	0.43	97	5.78	162	5.69	182
		g4-1	32	0.66	42	0.73	108	1.33			69
		g4-2	33	0.58	45	0.68	122	2.10			85
		g4-3	36	0.78	42	0.78	84	0.51			52
		g6-1	35	0.73	46	0.89	72	0.41			51
		g6-2	37	0.83	43	0.88	94	1.12			72
Shx4	0.306	g2-1 (R)	27	0.51	56	1.74	102	1.02			77
		g2-2 (M)	17	0.19	70	2.20	66	0.40			66
		g2-3 (C)	16	0.16	69	2.08	66	0.36			61
		g2-4 (M)	17	0.20	62	1.82	61	0.33			55
		g2-5 (R)	12	0.14	71	2.42	67	0.45			71
		g5-1	34	1.00	52	1.72	110	2.18			115
		g5-2	38	0.99	44	1.00	94	1.26			76
		g5-3	40	1.05	42	0.86	100	1.01	62	0.25	69
		g5-4	37	0.95	45	1.05	72	0.45			58
		g9-1 (M)	51	2.39	35	0.85	69	0.72			93
		g9-2 (C)	34	1.30	39	1.15	76	0.41			67
		g9-3 (M)	34	1.49	38	1.25	67	0.40			74
Shx7	0.264	g1-1 (C)	26	8.46	58	56.30					1765
		g1-2 (M)	26	8.49	58	58.72					1832

(continued)

TABLE 1. (*contd.*)

			Group I		Group II		Group III		Group IV		
			3635–3655 cm^{-1}		3600–3630 cm^{-1}		3540–3580 cm^{-1}		3400–3450 cm^{-1}		
Sample	Thickness (mm)	Spot	FWHH	Area	FWHH	Area	FWHH	Area	FWHH	Area	Water Content (ppm)
		g1-3 (R)	35	21.30	49	42.50					1739
		g1-4 (M)	27	9.04	58	58.77					1848
		g1-5 (R)	26	8.54	59	59.79					1862
		g2-1 (R)	31	17.30	55	52.50					1902
		g2-2 (M)	30	16.44	55	55.54					1962
		g2-3 (C)	31	17.52	55	60.29					2120
		g2-4 (M)	31	16.43	55	62.61					2154
		g6-1 (M)	26	7.50	58	57.51					1772
		g6-2 (C)	34	19.67	49	41.98					1680
		g6-3 (M)	26	6.88	59	54.14					1663
		g6-4 (M)	28	8.99	57	56.44					1783
		g6-5 (R)	27	8.34	57	55.83					1749
Shx8	0.290	g2-1 (M)	36	30.21	51	56.14					2142
		g2-2 (C)	32	17.72	56	67.79					2121
		g2-3 (M)	27	10.17	60	79.48					2224
Shx9	0.314	g1-2 (M)	33	19.17	62	50.32					1592
		g1-3 (C)	34	20.57	63	52.52					1675
		g1-4 (M)	30	12.83	57	47.39					1380
		g2-1			63	68.10					1560
		g2-2			64	62.61					1434
Shx13	0.249	g1-1 (R)	40	29.20	47	31.13					1743
		g1-2 (M)	26	8.28	59	52.42					1754
		g1-3 (C)	27	8.88	58	54.71					1837
		g1-4 (M)	26	8.12	59	58.01					1911
		g2-1 (R)	27	10.23	60	67.43					2244
		g2-2 (M)	27	10.17	59	70.05					2318
		g2-3 (C)	28	11.81	60	75.73					2529
		g2-4 (M)	27	9.44	60	64.80					2145
		g2-5 (R)	27	9.72	60	61.07					2045
		g6-1	38	29.14	45	35.97					1881
		g6-2	37	26.91	45	35.53					1804
		g6-3	36	25.42	47	40.48					1904
		g6-4	26	8.28	59	60.48					1987

		g6-5	36	19.19	47	36.77					1617
Shx15	0.226	g3-1			91	17.98	66	9.87	237	43.06	887
		g3-2	42	4.11	35	2.87	84	7.43	183	9.55	459
		g3-3			93	22.27	67	18.99	219	62.86	1313
		g3-4	56	5.68	33	1.84	77	7.09	244	16.54	465
Shx17	0.244	g3-1 (R)	28	5.48	63	28.63					1006
		g3-2 (M)	28	5.85	61	24.59					898
		g3-3 (C)	28	5.56	61	23.86					867
		g3-4 (M)	28	4.92	60	26.80					935
		g3-5 (R)	28	6.57	59	29.30					1058
		g3-6 (R)	27	5.83	61	30.22					1063
		g4-1 (R)	25	3.33	61	25.14					839
		g4-2 (M)	26	3.83	60	23.05					793
		g4-3 (C)	27	3.94	60	22.58					782
		g4-4 (M)	28	4.39	61	20.88					745
		g4-5 (R)	28	3.91	61	16.75					609
		g4-6 (R)	28	3.67	61	17.36					620
		g4-7 (R)	28	4.86	62	21.54					778
Shx18	0.303	g2-1 (C)	27	6.68	61	35.79					1008
		g2-2 (M)	27	6.96	61	36.24					1026
		g2-3 (M)	28	7.18	61	35.40					1011
		g2-4 (R)	29	7.40	63	35.64					1022
		g3-1 (R)	28	6.76	60	27.48					813
		g3-2 (M)	28	6.47	60	28.06					820
		g3-3 (C)	28	6.50	61	29.12					846
		g3-4 (M)	29	8.07	63	31.32					935
		g3-5 (R)	29	7.39	63	30.70					904

(1) C: Core, M: Mantle, R: Rim and 'other spots' is generally in the core or mantle of garnets grain.
(2) FWHH (cm^{-1}) and Area (Area·cm^{-2}) of each band were obtained by Gaussian fit after baseline correction.
(3) Structural water content was calculated by the Beer-Lambert law using the absorption area of the first three band groups. The group IV bands that most probably originate from submicroscopic fluid inclusions (see text) were not included in the structural water calculation.

TABLE 2. The composition of garnets from UHP eclogites at Shuanghe, Dabieshan.

Sample	Shw2	Shx1				Shx4					Shx7				Shx8	Shx9	
Spot	g1-3	g1-1	g2-1	g4-3	g6-2	g2-2	g2-3	g5-2	g5-3	g9-2	g1-1	g1-2	g1-5	g6-2	g2-2	g1-2	g2-2
SiO_2	39.57	38.50	38.25	38.50	38.58	39.47	38.75	39.61	39.65	39.05	39.85	39.86	39.43	39.22	38.57	39.29	39.23
TiO_2	0.00	0.00	0.00	0.01	0.00	0.00	0.01	0.00	0.02	0.00	0.00	0.00	0.02	0.14	0.02	0.03	0.05
Al_2O_3	22.22	22.43	21.75	21.75	21.60	22.05	21.16	22.26	22.07	21.99	22.37	22.62	22.48	21.94	21.94	21.85	21.67
FeO	20.32	25.97	26.04	25.32	25.32	22.34	21.79	22.41	22.85	23.15	18.75	19.07	19.40	18.90	20.35	21.38	21.03
MnO	0.23	0.30	0.29	0.53	0.53	0.32	0.24	0.19	0.26	0.21	0.50	0.29	0.49	0.33	0.52	0.44	0.28
MgO	4.63	4.88	4.64	4.55	4.79	4.55	4.95	4.67	4.84	4.97	4.32	3.81	3.98	4.38	3.56	3.77	3.56
CaO	12.90	7.85	9.23	9.34	9.44	11.81	12.49	11.14	11.20	10.51	15.18	15.90	15.12	14.89	14.26	14.00	13.46
Na_2O	0.00	0.00	0.00	0.00	0.00	0.00	0.00	0.00	0.00	0.00	0.00	0.00	0.00	0.01	0.00	0.00	0.01
K2O	0.00	0.00	0.00	0.00	0.00	0.00	0.00	0.00	0.00	0.00	0.00	0.00	0.00	0.00	0.00	0.00	0.00
Cr_2O_3	0.00	0.00	0.00	0.00	0.00	0.00	0.00	0.00	0.00	0.00	0.00	0.00	0.00	0.00	0.00	0.00	0.00
H_2O	0.008	0.005	0.011	0.007*	0.007	0.007	0.006	0.008	0.007	0.007	0.177	0.183	0.186	0.168	0.212	0.155*	0.143
Total	99.88	99.92	100.22	100.01	100.27	100.54	99.40	100.29	100.88	99.89	101.15	101.73	101.10	99.97	99.43	100.92	99.41
Atoms per 12 O																	
Si	3.037	2.994	2.978	3.002	2.998	3.030	3.013	3.039	3.033	3.019	3.014	3.004	2.994	3.006	2.992	3.010	3.040
Ti	0.000	0.000	0.000	0.001	0.000	0.000	0.001	0.000	0.001	0.000	0.000	0.000	0.001	0.008	0.001	0.002	0.003
Al	2.010	2.056	1.996	1.999	1.978	1.995	1.939	2.013	1.989	2.004	1.994	2.009	2.012	1.982	2.006	1.973	1.979
Fe^{2+}	1.304	1.689	1.652	1.651	1.623	1.434	1.385	1.438	1.461	1.497	1.186	1.202	1.232	1.212	1.320	1.369	1.363
Fe^{3+}	0.000	0.000	0.044	0.000	0.023	0.000	0.032	0.000	0.000	0.000	0.000	0.000	0.000	0.000	0.000	0.000	0.000
Mn^{2+}	0.015	0.019	0.019	0.035	0.035	0.021	0.016	0.012	0.017	0.014	0.032	0.019	0.031	0.021	0.034	0.029	0.018
Mg	0.529	0.565	0.539	0.528	0.555	0.521	0.574	0.534	0.551	0.573	0.488	0.428	0.451	0.500	0.412	0.431	0.411
Ca	1.061	0.654	0.770	0.780	0.786	0.971	1.040	0.916	0.918	0.870	1.230	1.284	1.230	1.223	1.185	1.149	1.117
Na	0.000	0.000	0.000	0.000	0.000	0.000	0.000	0.000	0.000	0.000	0.000	0.000	0.000	0.001	0.000	0.000	0.001
Cr	0.000	0.000	0.000	0.000	0.000	0.000	0.000	0.000	0.000	0.000	0.000	0.000	0.000	0.000	0.000	0.000	0.000
H_4	0.001	0.001	0.001	0.001	0.001	0.001	0.001	0.001	0.001	0.001	0.022	0.023	0.024	0.021	0.027	0.020	0.019

(*continued*)

TABLE 2. (*contd.*)

Sample	Shx13										Shx15	Shx17		Shx18				
Spot	g1-2	g1-3	g1-4	g2-1	g2-2	g2-3	g2-4	g2-5	g6-3	g6-4	g3-4	g3-3	g4-2	g2-4	g3-1	g3-2	g3-3	g3-4
SiO_2	39.03	38.85	39.20	39.29	39.06	39.16	39.29	39.27	39.24	38.89	40.04	39.43	38.68	39.60	39.53	39.49	39.83	39.80
TiO_2	0.00	0.05	0.01	0.00	0.00	0.00	0.04	0.00	0.00	0.04	0.00	0.03	0.03	0.02	0.00	0.00	0.00	0.00
Al_2O_3	21.98	21.93	22.30	22.18	22.04	21.87	22.08	21.93	21.65	21.43	21.83	22.20	22.12	21.85	22.03	22.19	22.33	22.22
FeO	21.05	20.79	21.11	20.37	20.99	19.82	18.52	21.52	21.79	21.59	22.23	21.33	20.91	22.04	21.20	21.40	22.10	21.38
MnO	0.30	0.15	0.26	0.23	0.25	0.28	0.27	0.29	0.33	0.45	0.90	0.28	0.17	0.28	0.27	0.26	0.23	0.23
MgO	3.25	3.69	3.07	4.12	3.15	3.78	3.90	3.61	3.29	3.33	6.26	4.10	3.79	3.87	4.06	4.35	4.27	4.24
CaO	13.49	14.23	14.00	13.76	15.33	15.39	15.31	14.40	14.25	14.84	8.97	12.20	13.90	13.66	13.24	13.34	13.15	13.23
Na_2O	0.00	0.00	0.00	0.00	0.00	0.00	0.00	0.00	0.00	0.00	0.00	0.00	0.00	0.00	0.00	0.00	0.00	0.00
K_2O	0.00	0.00	0.00	0.00	0.00	0.00	0.00	0.00	0.00	0.00	0.00	0.00	0.00	0.00	0.00	0.00	0.00	0.00
Cr_2O_3	0.00	0.00	0.00	0.00	0.00	0.00	0.00	0.00	0.00	0.00	0.00	0.00	0.08	0.00	0.00	0.00	0.00	0.00
H_2O	0.175	0.184	0.191	0.224	0.232	0.253	0.215	0.205	0.190	0.199	0.047	0.087	0.079	0.102	0.081	0.082	0.085	0.094
Total	99.27	99.87	100.13	100.18	101.06	100.55	99.63	101.21	100.73	100.76	100.27	99.64	99.75	101.42	100.41	101.11	101.98	101.18
Atoms per 12 O																		
Si	3.028	2.999	3.017	3.010	2.990	2.998	3.016	3.001	3.017	2.997	3.058	3.039	2.994	3.022	3.031	3.011	3.015	3.028
Ti	0.000	0.003	0.000	0.000	0.000	0.000	0.002	0.000	0.000	0.002	0.000	0.002	0.002	0.001	0.000	0.000	0.000	0.000
Al	2.010	1.996	2.023	2.003	1.989	1.973	1.997	1.975	1.962	1.946	1.965	2.016	2.018	1.965	1.992	1.994	1.992	1.992
Fe^{2+}	1.366	1.342	1.358	1.305	1.344	1.268	1.189	1.375	1.401	1.387	1.420	1.375	1.354	1.406	1.360	1.365	1.399	1.360
Fe^{3+}	0.000	0.000	0.000	0.000	0.000	0.000	0.000	0.000	0.000	0.004	0.000	0.000	0.000	0.000	0.000	0.000	0.000	0.000
Mn^{2+}	0.020	0.010	0.017	0.015	0.016	0.018	0.018	0.019	0.022	0.030	0.058	0.018	0.011	0.018	0.018	0.017	0.015	0.015
Mg	0.376	0.425	0.352	0.471	0.359	0.432	0.447	0.411	0.377	0.382	0.712	0.471	0.437	0.441	0.464	0.494	0.481	0.480
Ca	1.122	1.177	1.154	1.129	1.258	1.263	1.259	1.179	1.174	1.226	0.734	1.007	1.153	1.117	1.088	1.090	1.066	1.078
Na	0.000	0.000	0.000	0.000	0.000	0.000	0.000	0.000	0.000	0.000	0.000	0.000	0.000	0.000	0.000	0.000	0.000	0.000
Cr	0.000	0.000	0.000	0.000	0.000	0.000	0.000	0.000	0.000	0.000	0.000	0.000	0.005	0.000	0.000	0.000	0.000	0.000
H_4	0.023	0.024	0.025	0.029	0.030	0.032	0.027	0.026	0.024	0.026	0.006	0.011	0.010	0.013	0.010	0.010	0.011	0.012

The EMPA analysis spots are consistent with the FTIR analysis, and the formula calculation is based on 12 oxygen atoms.
H_2O content estimated from FTIR analysis. *: The average water content of the garnets grain.

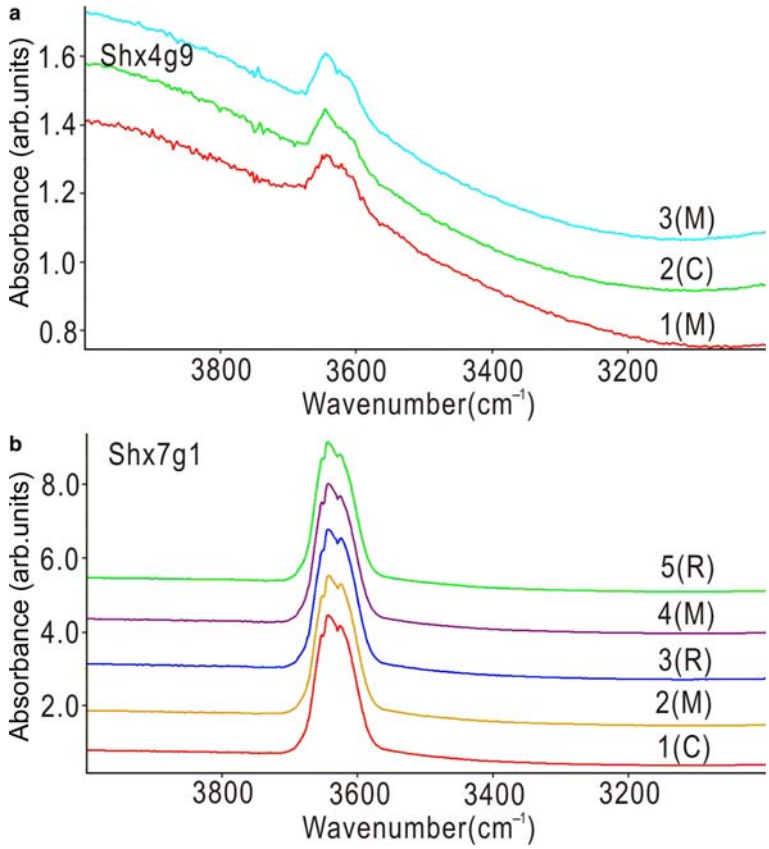

FIG. 3. Representative IR spectra (*a*, *b*; normalized to 1 mm; C: Core, M: Mantle, R: Rim) and its fitted result (*c*, *d*) of garnets from UHP eclogites at Shuanghe, Dabieshan.

and Rossman, 1993; Beran *et al.*, 1993; Xia *et al.*, 2005). In contrast, several spectra have group IV bands, and these are much broader. These bands are typical of the stretching vibrations of molecular water, which can occur in submicroscopic fluid inclusions in garnets. The results of this study are consistent with previous investigations of natural and synthesized garnets (Keppler and Smyth, 2006; Steven and Suzan, 2006).

The water content (H_2O ppm wt.) of garnet was calculated by the Beer-Lambert law (absorbance = absorption coefficient × thickness × water content). Absorbance is expressed as the integrated absorption of OH^-; the integrated molar absorption coefficient is from Bell *et al.* (1995): 1.39 ppm H_2O cm^{-2}. The thickness of the samples was measured by a micrometer. As we interpreted the group IV band and the 3710 cm^{-1} band to be caused by submicroscopic fluid inclusions and vapour, respectively, they were not included in the total integrated absorbance used for structural water content calculation. The amount of H_2O corresponding to the intrinsic hydroxyl contents of garnets from Shuanghe UHP eclogites ranges from 45 to 2529 ppm (Fig. 4).

The results show that the water contents are heterogeneous among the different grains of the same sample and within different zones of the same grain, but the trend of variation from core to rim differs from one garnet grain to another (Fig. 5). The water contents of different samples vary substantially and can be divided into two classes: (1) Shw2, Shx1 and Shx4 have low water content, with 45–398 ppm; (2) Shx7, Shx8, Shx9, Shx13, Shx15, Shx17 and Shx18 have high water content, with 459–2529 ppm.

https://doi.org/10.1180/minmag.2016.080.034 Published online by Cambridge University Press

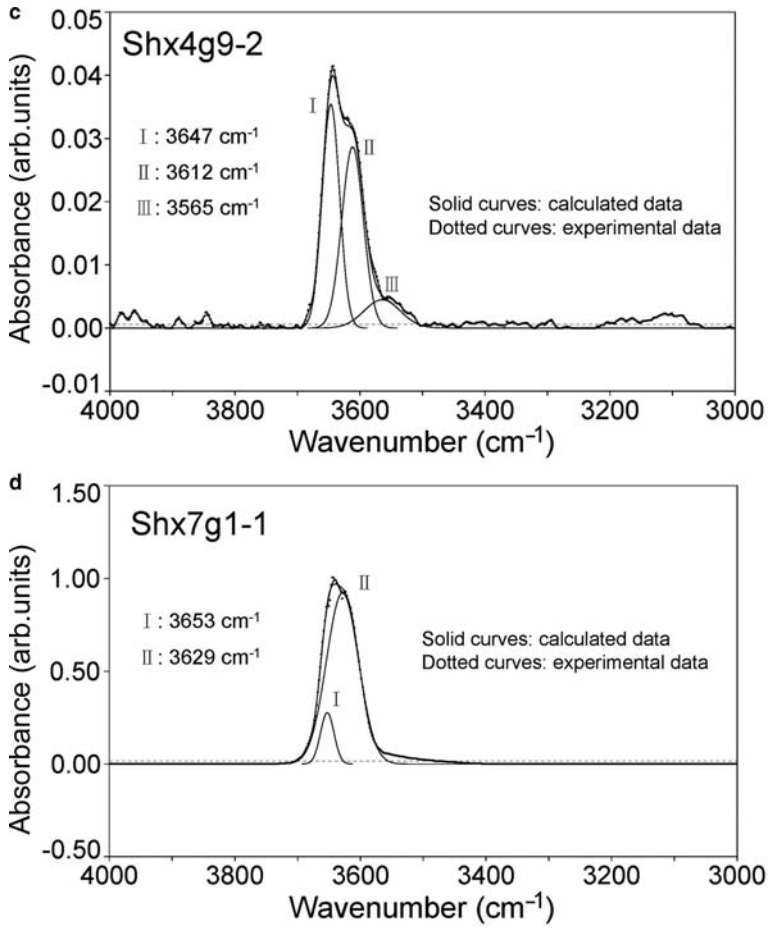

FIG. 3. Continued

Compositions of garnets

In order to determine the relationship between the water content and the chemical composition of garnets, based on the FTIR analysis results, 21 garnet grains (35 spots) with different water contents were investigated *in situ* by EMPA. The composition of garnets is given in Table 2, and cations per formula unit were calculated using the Excel spreadsheet of Grew *et al.* (2013) (Supplementary file 3).

The EMPA results showed that the major-oxide composition (such as SiO_2, FeO, Al_2O_3, MnO, MgO and CaO) is homogenous among different grains in the same sample and that there is no obvious compositional zoning within the same grain (Table 2), although there is a little heterogeneity among the different samples, and these data are consistent with previous studies (Cong *et al.*, 1995; Xu *et al.*, 1999; Liu *et al.*, 2006; Wang *et al.*, 2010).

Discussion

The OH incorporation in garnets

The water content of garnet shows an obvious positive correlation with Ca and a negative correlation with Si, Fe^{2+} and Mg per 12 O anions, and this relationship is more evident where the water content is >400 ppm, but there is no obvious relationship between water content and the atoms of Al and Mn (Fig. 6). This trend has been also shown in some previous studies, in the case of pyrope-rich garnets from UHP metamorphic rocks; mantle-

https://doi.org/10.1180/minmag.2016.080.034 Published online by Cambridge University Press

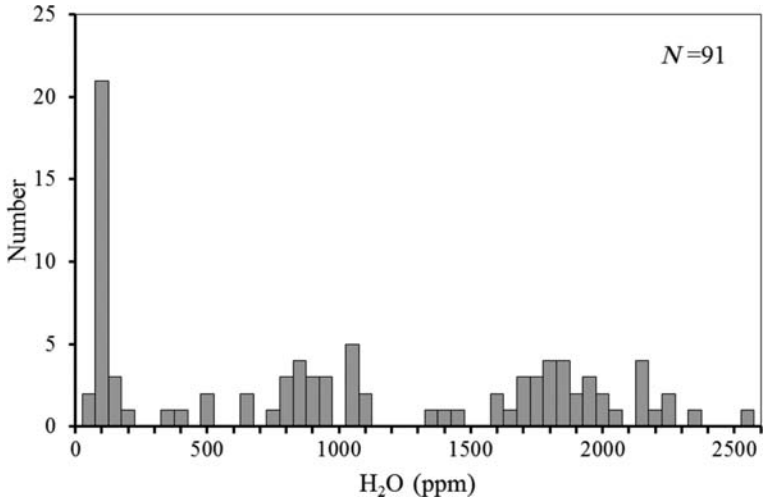

FIG. 4. Distribution of the water content of garnets from Shuanghe eclogites.

derived xenoliths; and high-pressure-temperature synthesized samples; mostly in samples with water content <200 ppm but in a few cases, in samples with as much as 1000 ppm H_2O (Ackermann *et al.*, 1983; Aines and Rossman, 1984*a*,*c*; Geiger *et al.*, 1991; Bell and Rossman, 1992; Lu and Keppler, 1997; Withers *et al.*, 1998; Mookherjee and Karato, 2010). In contrast, the grossular- or andradite-rich garnets generally have a higher water content of >600 ppm (Lager *et al.*, 1989; Beran *et al.*, 1993; Maldener *et al.*, 2003). Based on the FTIR and other analytical methods, many of the naturally occurring garnets containing substantial amounts of the hydroxyl ion have compositions intermediate between grossular (x = 0) and katoite (x = 3), i.e. $\{Ca_3\}[Al_2](Si_{3-x}\square_x)O_{12-4x}(OH)_{4x}$ where $0 < x < 3$ and $\square$ is a vacancy, and for the majority of these garnets, $x < 1.5$ (Grew *et al.*, 2013). Thus, the major

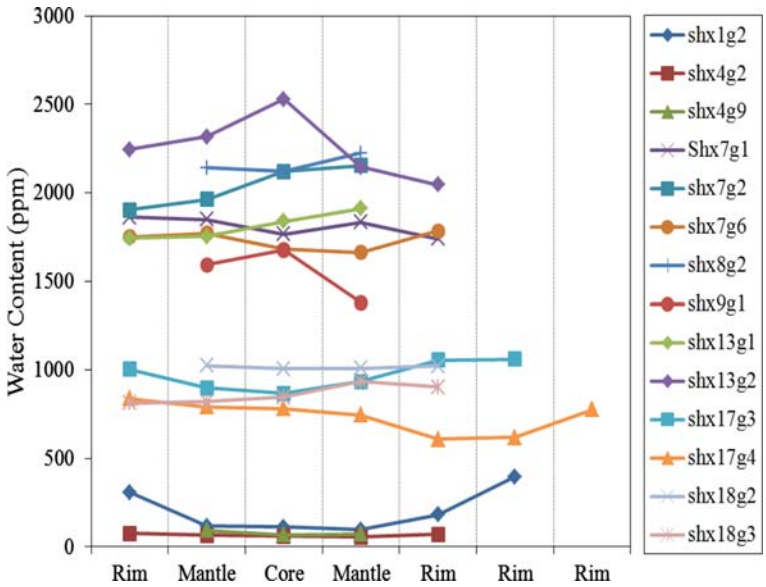

FIG. 5. The distribution of water content in the same garnet grain.

https://doi.org/10.1180/minmag.2016.080.034 Published online by Cambridge University Press

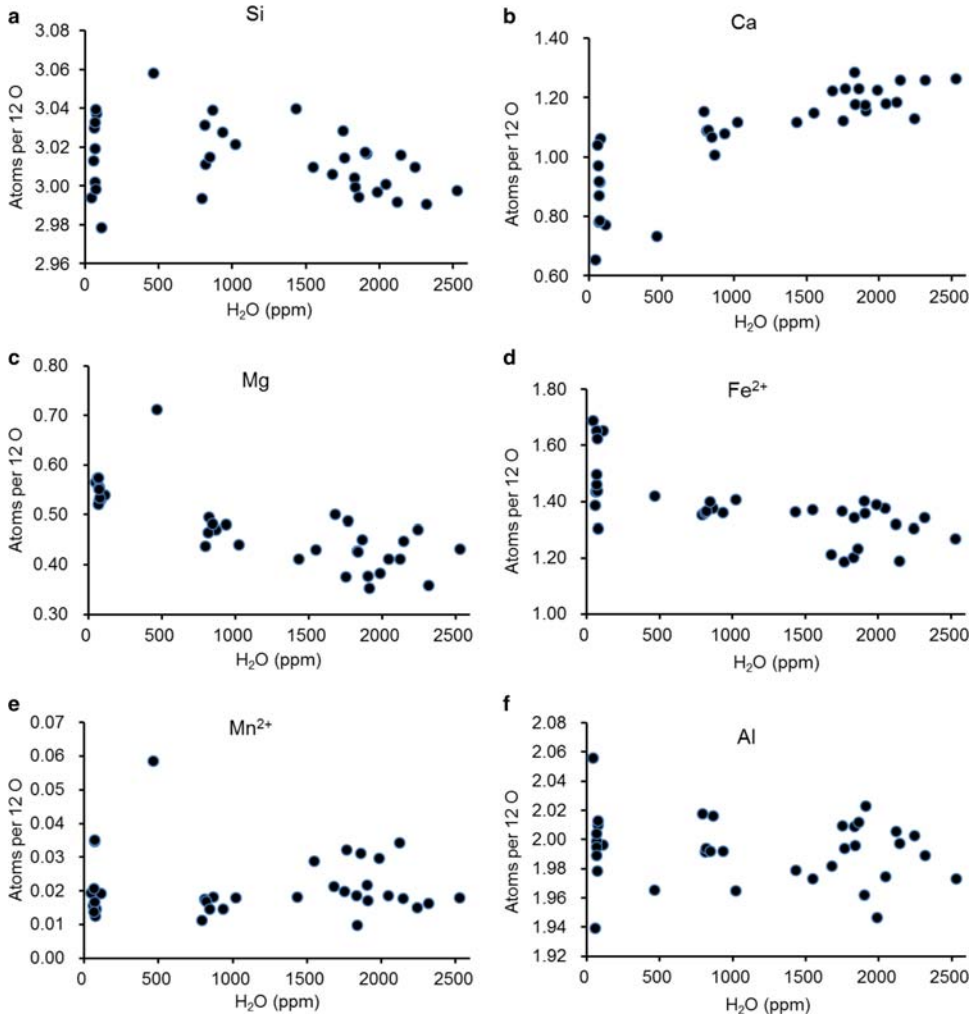

FIG. 6. The relationship between water content and composition of garnets from UHP eclogites at Shuanghe, Dabieshan.

mechanism of hydroxyl incorporation in garnet is by the coupled substitution $4H + {}^{Z}\square \rightarrow \square + {}^{Z}Si$ at the tetrahedral site, but significant incorporation of OH by this substitution is limited mostly to garnet in which the *X* site is occupied by Ca, i.e. katoite, holtstamite and henritermierite. In summary, the H_2O contents of natural and synthetic garnets are consistent with the conclusion reached by Lager *et al.* (1989) that the extent of OH substitution in garnets appears to be controlled structurally, i.e. it is greater, when the effective ionic radius of the *X*-site cation exceeds 1.0 Å and the shared octahedral edge is longer than the unshared edge, which is the case for natural and synthetic garnets with Ca dominant at the *X* site (Novak and Gibbs, 1971; Quartieri *et al.*, 2006). This is an expected behaviour as, on the basis of ionic radii, magnesium is generally considered to be too small to occupy the large dodecahedron, even in anhydrous pyrope. An expansion of the pyrope structure caused by the hydrogarnet substitution is thus energetically unfavourable, as it involves an increase in the size of the dodecahedron. It was found that the hydrogarnet substitution in pyrope requires 186 kJ mol^{-1} more energy than in grossular, so that katoite is significantly more stable than a

https://doi.org/10.1180/minmag.2016.080.034 Published online by Cambridge University Press

hypothetical Mg-analogue of katoite. In addition, a rough estimate of the formation energy of these two hydrogarnets suggests that its value is close to zero for katoite and close to –180 kJ mol^{-1} for the Mg analogue of katoite. These results show that the expansion of the dodecahedral site due to the hydrogarnet substitution can only be sustained when the anhydrous structure contains a large divalent cation (e.g. calcium) in the *X* site and a small trivalent cation in the *Y* site. This implies that none of the known pyrope- and majorite-rich garnet in the deep earth are likely to exhibit a stable and significant hydrogarnet substitution as the ratio of ionic radii of *X*-site to *Y*-site cations is less in pyrope- and majorite-rich garnet than in grossular (Aines and Rossman, 1984*a*; Lager *et al.*, 1989; Milman *et al.*, 2000; Thomas *et al.*, 2015).

Based on the OH absorption band behaviour of the first three groups and the relationship between water content and composition, we conclude that the OH in garnets containing >400 ppm H_2O was incorporated by $4H + {}^{Z}\square \rightarrow \square + {}^{Z}Si$ at the tetrahedral site (Aines and Rossman, 1984*c*; Beran *et al.*, 1993; Beran and Libowitzky, 2003; Birkett and Trzcienski, 1984; Rossman and Aines, 1991).

However, garnets containing ≤400 ppm H_2O show no obvious linear correlation between water content and composition, the OH incorporation mechanism seems more complicated (Andrut and Wildner, 2001; Andrut *et al.*, 2002; Johnson, 2003; Cho and Rossman, 1993; Khomenko *et al.*, 1994). In Ti-bearing garnets there is a possible substitution of Ti^{4+} by Al^{3+} in close proximity to the tetrahedral (vacant) site, which is replaced by an incomplete cluster of $[(OH)_3O]^{5-}$ (Andrut *et al.*, 2002; Johnson, 2003; Khomenko *et al.*, 1994). A study of birefringent natural uvarovite garnets concluded that $SiO_3(OH)$ tetrahedral groups are an important mechanism of OH defects in garnets with low water content (Andrut and Wildner, 2001; Andrut *et al.*, 2002).

Geological implications

The high water content and how it is incorporated into garnets from the Shuanghe eclogites have the following geological implications:

(1) The high water content indicates that it is an important mineral for recycling surface water into the mantle during the bulk processes of continental subduction and exhumation. The water contents of garnets from the Shuanghe eclogites range from 45 to 2529 ppm, and the major mechanism of hydroxyl incorporation in garnet is by the coupled substitution $4H + {}^{Z}\square \rightarrow \square + {}^{Z}Si$ at the tetrahedral site. Although the water content in garnet is much less than that of minerals containing essential water, garnet is potentially a significant water reservoir in the Earth's mantle as it is relatively abundant. Based on the above analysis, the OH in garnets is present in the form of hydrogrossular substitution (Aines and Rossman, 1984*c*; Beran *et al.*, 1993; Beran and Libowitzky, 2003; Rossman and Aines, 1991).

(2) Many studies have shown that under high-temperature and -pressure conditions water can significantly influence physical and chemical properties of garnets, such as melting temperature, electrical conductivity, fluid activity, mineral-phase transitions, rheological properties, and plastic deformation mechanisms (see for instance, Keppler and Smyth, 2006). Our study shows that garnet could contain few thousand ppm of water providing strong evidence of water participation in the processes of metamorphism and deformation of garnets under high temperature and high pressure (Beran and Libowitzky, 2006; Johnson, 2006; Su *et al.*, 2002*a*). Water can facilitate dislocation glide (Liu *et al.*, 2005; Su *et al.*, 2002*a*,*b*) as well as diffusion and grain boundary glide (Wang and Ji, 2000; Zhang and Green, 2007), all of which enhance deformation of garnet. The eclogites from Shuanghe in this study are foliated eclogites and the garnets are obviously elongated, indicating that the garnets have experienced plastic deformation. According to the temperature conditions of garnet plastic deformation, this process occurs in the coesite eclogite facies (Xu *et al.*, 1999).

Conclusion

(1) The FTIR analytical results show that all of the garnets from the Shuanghe UHP eclogite have more than two absorption bands between ~3000–4000 cm^{-1}. The OH absorption bands can be divided into four groups: (I) 3635–3655 cm^{-1}; (II) 3600–3630 cm^{-1}; (III) 3540–3580 cm^{-1}; and (IV) 3400–3450 cm^{-1} – the first three groups result from the garnet OH-stretching vibration and water content ranging from 45 to 2529 ppm, whereas group IV is caused by H_2O, in grain boundaries or submicroscopic fluid inclusions. (2) The water content of garnet shows an obvious positive correlation with Ca and a negative correlation with Si, Fe^{2+} and Mg per 12 O anions, and this relationship is more evident when the water content is >400 ppm. It is concluded

https://doi.org/10.1180/minmag.2016.080.034 Published online by Cambridge University Press

that the major mechanism of hydroxyl incorporation in garnet is by the coupled substitution $4H + {}^{Z}\square \rightarrow \square + {}^{Z}Si$ at the tetrahedral site; as a result, grossular-rich garnet is potentially a significant reservoir of water in the Earth's mantle.

Acknowledgements

The authors thank Dr. Shi Feng for his help with FTIR analysis, and Liu Hui-fang for assistance with EMPA analysis. This work was supported by National Natural Science Foundation of China (Grant No. 40872136, Grant No. 41272224).

References

Ackermann, L., Cemič, L. and Langer, K. (1983) Hydrogarnet substitution in pyrope – a possible location for water in the mantle. *Earth and Planetary Science Letters*, **62**, 208–214.

Aines, R.D. and Rossman, G.R. (1984*a*) The hydrous component in garnets – pyralspites. *American Mineralogist*, **69**, 1116–1126.

Aines, R.D. and Rossman, G.R. (1984*b*) Water in minerals – a peak in the infrared. *Journal of Geophysical Research*, **89**, 4059–4071.

Aines, R.D. and Rossman, G.R. (1984*c*) Water content of mantle garnet. *Geology*, **12**, 720–723.

Andrut, M. and Wildner, M. (2001) The crystal chemistry of birefringent natural uvarovites: Part I. Optical investigations and UV-VIS-IR absorption spectroscopy. *American Mineralogist*, **86**, 1219–1230.

Andrut, M., Wildner, M. and Beran, A. (2002) The crystal chemistry of birefringent natural uvarovites. Part IV. OH defect incorporation mechanisms in non-cubic garnets derived from polarized IR spectroscopy. *European Journal of Mineralogy*, **14**, 1019–1026.

Armbruster, T., Birrer, J., Libowitzky, E. and Beran, A. (1998) Crystal chemistry of Ti-bearing andradites. *European Journal of Mineralogy*, **10**, 907–921.

Armbruster, T., Kohler, T., Libowitzky, E., Friedrich, A., Miletich, R., Kunz, M., Medenbach, O. and Gutzmer, J. (2001) Structure, compressibility, hydrogen bonding and dehydration of the tetragonal Mn^{3+} hydrogarnet, henritermierite. *American Mineralogist*, **86**, 147–158.

Bell, D.R. and Rossman, G.R. (1992) The distribution of hydroxyl in garnets from the subcontinental mantle of southern Africa. *Contributions to Mineralogy and Petrology*, **111**, 161–178.

Bell, D.R., Ihinger, P.D. and Rossman, G.R. (1995) Quantitative-analysis of trace OH in garnet and pyroxenes. *American Mineralogist*, **80**, 465–474.

Beran, A. and Libowitzky, E. (2003) IR spectroscopic characterization of OH defects in mineral phases. *Phase Transitions*, **76**, 1–15.

Beran, A. and Libowitzky, E. (2006) Water in natural mantle minerals II: Olivine, garnet and accessory minerals. *Water in Nominally Anhydrous Minerals*, **62**, 169–191.

Beran, A., Langer, K. and Andrut, M. (1993) Single-crystal Infrared-spectra in the range of OH fundamentals of paragenetic garnet, omphacite and kyanite in an eklogitic mantle xenolith. *Mineralogy and Petrology*, **48**, 257–268.

Birkett, T.C. and Trzcienski, W.E. (1984) Hydrogarnet – multi-site hydrogen occupancy in the garnet structure. *The Canadian Mineralogist*, **22**, 675–680.

Blanchard, M. and Ingrin, J. (2004) Kinetics of deuteration in pyrope. *European Journal of Mineralogy*, **16**, 567–576.

Cho, H. and Rossman, G.R. (1993) Single-crystal NMR studies of low-concentration hydrous species in minerals; grossular garnet. *American Mineralogist*, **78**, 1149–1164.

Cong, B., Zhai, M.G., Carswell, D.A., Wilson, R.N., Wang, Q.C., Zhao, Z.Y. and Windley, B.F. (1995) Petrogenesis of ultrahigh-pressure rocks and their country rocks at Shuanghe in Dabieshan, central China. *European Journal of Mineralogy*, **7**, 119–138.

Ferro, O., Galli, E., Papp, G., Quartieri, S., Szakall, S. and Vezzalini, G. (2003) A new occurrence of katoite and re-examination of the hydrogrossular group. *European Journal of Mineralogy*, **15**, 419–426.

Foreman, D.W. (1968) Neutron and X-ray diffraction study of $Ca_3Al_2(O4D_4)_3$, a garnetoid. *Journal of Chemical Physics*, **48**, 3037–3041.

Geiger, C.A. (2013) Garnet: A key phase in nature, the laboratory, and technology. *Elements*, **9**, 447–452.

Geiger, C.A., Langer, K., Bell, D.R., Rossman, G.R. and Winkler, B. (1991) The hydroxide component in synthetic pyrope. *American Mineralogist*, **76**, 49–59.

Grew, E.S., Locock, A.J., Mills, S.J., Galuskina, I.O., Galuskin, E.V. and Hålenius, U. (2013) Nomenclature of the garnet supergroup. *American Mineralogist*, **98**, 785–811.

Hålenius, U., Haussermann, U. and Harryson, H. (2005) Holtstamite, $Ca_3(Al,Mn^{3+})_2(SiO_4)_{3-x}(H_4O_4)_x$, a new tetragonal hydrogarnet from Wessels Mine, South Africa. *European Journal of Mineralogy*, **17**, 375–382.

Ingrin, J. and Skogby, H. (2000) Hydrogen in nominally anhydrous upper-mantle minerals: concentration levels and implications. *European Journal of Mineralogy*, **12**, 543–570.

Johnson, E.A. (2003) *Hydrogen in nominally anhydrous crustal minerals.* PhD Thesis. California Institute of Technology, California, USA.

Johnson, E.A. (2006) Water in nominally anhydrous crustal minerals: Speciation, concentration, and geologic significance. *Water in Nominally Anhydrous Minerals*, **62**, 117–154.

Kalinichenko, A.M., Proshko, V.Y., Matyash, I.C. and Pavlishin, Y.I. (1987) NMR data on crystallochemical

https://doi.org/10.1180/minmag.2016.080.034 Published online by Cambridge University Press

features of hydrogrossular. *Geochemistry International*, **24**, 132–135.

Keppler, H. and Smyth, J. (editors) (2006) *Water in Nominally Anhydrous Minerals.* Reviews in Mineralogy & Geochemistry, **62**. Mineralogical Society of America and the Geochemical Society, Chantilly, Virginia, USA, 478 pp.

Khomenko, V.M., Langer, K., Beran, A., Kochmuller, M. and Fehr, T. (1994) Titanium substitution and OH-bearing defects in hydrothermally grown pyrope crystals. *Physics and Chemistry of Minerals*, **20**, 483–488.

Kurka, A., Blanchard, M. and Ingrin, J. (2005) Kinetics of hydrogen extraction and deuteration in grossular. *Mineralogical Magazine*, **69**, 359–371.

Lager, G.A., Armbruster, T. and Faber, J. (1987) Neutron and X-ray-diffraction study of hydrogarnet $Ca_3Al_2(O_4H_4)_3$. *American Mineralogist*, **72**, 756–765.

Lager, G.A., Armbruster, T., Rotella, F.J. and Rossman, G.R. (1989) OH substitution in garnets – X-ray and Neutron-Diffraction, Infrared, and Geometric-Modeling studies. *American Mineralogist*, **74**, 840–851.

Li, S.G., Jagoutz, E., Chen, Y.Z. and Li, Q.L. (2000) Sm-Nd and Rb-Sr isotopic chronology and cooling history of ultrahigh pressure metamorphic rocks and their country rocks at Shuanghe in the Dabie Mountains, Central China. *Geochimica et Cosmochimica Acta*, **64**, 1077–1093.

Libowitzky, E. and Beran, A. (2006) The structure of hydrous species in nominally anhydrous minerals: Information from polarized IR spectroscopy. *Water in Nominally Anhydrous Minerals*, **62**, 29–52.

Liou, J.G., Zhang, R.Y. and Jahn, B. (1997) Petrology, geochemistry and isotope data on a ultrahigh-pressure jadeite quartzite from Shuanghe, Dabie mountains, east-central China. *Lithos*, **41**, 59–78.

Liu, F., Xue, H., Xu, Z., Liang, F. and Axel, G. (2006) SHRIMP U-Pb zircon dating from eclogite lens in marble, Shuanghe area, Dabie UHP terrane: restriction on the prograde, UHP and retrograde metamorphic ages. *Acta Petrologica Sinica*, **22**, 1761–1778.

Liu, X.W., Jin, Z.M., Jin, S.Y., Qu, J. and Xu, W. (2005) Differences of deformation characteristics of garnets from two types of eclogites: Evidence from TEM study. *Acta Petrologica Sinica*, **21**, 411–420.

Lu, R. and Keppler, H. (1997) Water solubility in pyrope to 100 kbar. *Contributions to Mineralogy and Petrology*, **129**, 35–42.

Maldener, J., Hosch, A., Langer, K. and Rauch, F. (2003) Hydrogen in some natural garnets studied by nuclear reaction analysis and vibrational spectroscopy. *Physics and Chemistry of Minerals*, **30**, 337–344.

Martin, R.F. and Donnay, G. (1972) Hydroxyl in the mantle. *American Mineralogist*, **57**, 554–570.

Milman, V., Winkler, B., Nobes, R.H., Akhmatskaya, E.V., Pickard, C.J. and White, J.A. (2000) Garnets: structure, compressibility, dynamics, and disorder. *Jom – Journal of the Minerals Metals & Materials Society*, **52**, 22–25.

Mookherjee, M. and Karato, S. (2010) Solubility of water in pyrope-rich garnet at high pressures and temperature. *Geophysical Research Letters*, **37**, 1–5.

Novak, G.A. and Gibbs, G.V. (1971) The crystal chemistry of the silicate garnets. *The American Mineralogist*, **56**, 791–825.

Quartieri, S., Oberti, R., Boiocchi, M., Dalconi, M.C., Boscherini, F., Safonova, O. and Woodland, A.B. (2006) Site preference and local geometry of Sc in garnets: Part II. The crystal-chemistry of octahedral Sc in the andradite–$Ca_3Sc_2Si_3O_{12}$ join. *American Mineralogist*, **91**, 1240–1248.

Rossman, G.R. (1996) Studies of OH in nominally anhydrous minerals. *Physics and Chemistry of Minerals*, **23**, 299–304.

Rossman, G.R. and Aines, R.D. (1991) The hydrous components in garnets – grossular-hydrogrossular. *American Mineralogist*, **76**, 1153–1164.

Sheng, Y.M., Xia, Q.K., Hao, Y.T., Wang, R.C. and Chen, X.M. (2005) Water in UHP Eclogites at Shuanghe, Dabieshan: Micro-FTIR Analysis. *Earth Science – Journal of China University of Geosciences*, **30**, 673–684.

Steven, D.J. and Suzan, V.D.L. (2006) *Earth's Deep Water Cycle.* American Geophysical Union, Washington DC, 313 pp.

Su, W., Cong, B.L., You, Z.D., Zhong, Z.Q. and Chen, D. Z. (2002*a*) Plastic mechanism of deformation of garnet – Water weakening. *Science in China Series D-Earth Sciences*, **45**, 885–892.

Su, W., You, Z.D., Cong, B.L., Ye, K. and Zhong, Z.Q. (2002*b*) Cluster of water molecules in garnet from ultrahigh-pressure eclogite. *Geology*, **30**, 611–614.

Thomas, S., Wilson, K., Koch-Müller, M., Hauri, E.H., McCammon, C., Jacobsen, S.D., Lazarz, J., Rhede, D., Ren, M., Blair, N. *et al.* (2015) Quantification of water in majoritic garnet. *American Mineralogist*, **100**, 1084–1092.

Wang, L., Jin, Z.M., Kusky, T., Xu, H.J. and Liu, X.W. (2010) Microfabric characteristics and rheological significance of ultra-high-pressure metamorphosed jadeite-quartzite and eclogite from Shuanghe, Dabie Mountains, China. *Journal of Metamorphic Geology*, **28**, 163–182.

Wang, Z.C. and Ji, S.C. (2000) Diffusion creep of fine-grained garnetite: implications for the flow strength of subducting slabs. *Geophysical Research Letters*, **27**, 2333–2336.

Wilkins, R.W.T. and Sabine, W. (1973) Water-content of some nominally anhydrous silicates. *American Mineralogist*, **58**, 508–516.

Withers, A.C., Wood, B.J. and Carroll, M.R. (1998) The OH content of pyrope at high pressure. *Chemical Geology*, **147**, 161–171.

https://doi.org/10.1180/minmag.2016.080.034 Published online by Cambridge University Press

Wright, K. (2006) Atomistic models of OH defects in nominally anhydrous minerals. *Water in Nominally Anhydrous Minerals*, **62**, 67–83.

Wright, K., Freer, R. and Catlow, C. (1994) The energetics and structure of the hydrogarnet defect in grossular – a computer-simulation study. *Physics and Chemistry of Minerals*, **20**, 500–503.

Xia, Q.K., Sheng, Y.M., Yang, X.Z. and Yu, H.M. (2005) Heterogeneity of water in garnets from UHP eclogites, eastern Dabieshan, China. *Chemical Geology*, **224**, 237–246.

Xu, S., Liu, Y., Su, W., Wu, W., Jiang, L. and Wang, R. (1999) Geometry, kinematics and tectonic implication of the deformed garnets in the foliated eclogite from the ultra-high pressure metamorphic belt in the Dabie Mountains, eastern China. *Acta Petrologica Sinica*, **15**, 321–337.

Xu, S., Wu, W., Liu, Y. and Wang, H. (2008) Metamorphic collisional melange in the Dabie mountains, eastern China. *Journal of Geomechanics*, **14**, 1–21.

Zhang, J.F. and Green, H.W. (2007) Experimental investigation of eclogite rheology and its fabrics at high temperature and pressure. *Journal of Metamorphic Geology*, **25**, 97–115.

Zhang, J.F., Jin, Z.M., Green, H.W. and Jin, S.Y. (2001) Hydroxyl in continental deep subduction zone: Evidence from UHP eclogites of the Dabie Mountains. *Chinese Science Bulletin*, **46**, 592–596.

Zhang, R.Y., Liou, J.G. and Ernst, W.G. (2009) The Dabie-Sulu continental collision zone: A comprehensive review. *Gondwana Research*, **16**, 1–26.

Zheng, Y.F. (2008) A perspective view on ultrahigh-pressure metamorphism and continental collision in the Dabie-Sulu orogenic belt. *Chinese Science Bulletin*, **53**, 3081–3104.

https://doi.org/10.1180/minmag.2016.080.034 Published online by Cambridge University Press